Mid-level clouds over the Sahara in a convection-permitting regional model

Damianos F. Mantsis[1], Steven Sherwood[1], Vishal Dixit[1],
Hugh Morrison[2] and Greg Thompson[2]

[1]*Climate Change Research Centre, University of New South Wales, Sydney, Australia*
[2]*Mesoscale and Microscale Meteorology Laboratory, National Center for Atmospheric Research, Boulder, Colorado, USA*

28 November, 2017

Corresponding Author: d.mantsis@unsw.edu.au

Abstract

The simulation of Saharan mid tropospheric clouds is investigated with the Weather Research and Forecasting (WRF) atmospheric model at convection permitting (4 km) horizontal grid-spacing in a regional configuration. We identify two potential problems in the simulations: one that affects cloud cover, and another that affects both the mean and geographic patterns of both cloud and precipitation. Our simulations show that using a vertical grid typical of GCMs (38 levels) limits the model's ability to simulate the Sahara mid-level clouds. In particular, it underestimates the supercooled liquid water (SLW) content that often resides at cloud top in mid-level clouds in favour of ice, which falls out of the cloud very quickly. It is only when the vertical resolution becomes high enough, allowing layers of SLW and ice to exist separately, that the simulation of the Saharan mid-level clouds becomes realistic. Additional improvement in the simulated clouds over the Sahel/Sahara is achieved by using a high resolution surface albedo forcing dataset derived from MODIS satellite, which shows that mid-level Saharan clouds prefer to form over areas of low albedo. Furthermore, realistic patterns of albedo are crucial to simulating the precipitation on the northern edge of the monsoon and the Sahel.

1. *Introduction*

Despite the West-African monsoon circulation having a zonally uniform nature, simulating it poses a number of challenges, including the potential importance of microphysical processes, boundary layer physics, and deep convection. Moreover, the region is bounded to the south and west by ocean and to the north by a vast desert. The zonal-mean cloud distribution is affected by all of these processes, and can be roughly divided into three distinct features. To the south, over the Gulf of Guinea, there are commonly shallow, non-precipitating stratiform clouds only a few hundred meters above the surface that penetrate inland as far as 10-15°N (Knippertz et al. 2011). Deep monsoonal convection that stretches throughout the atmospheric column occurs from 5-15°N with maximum cloud fraction in the upper troposphere (Stein et al. 2011). To the north of 15°N, over the warm and dry Sahel/Sahara region, convection becomes more sporadic and the cloud fraction is dominated by relatively thin mid-level cloud layers (Saharan mid-level clouds, SMLC), consisting mostly of altocumulus atop the very deep Saharan atmospheric boundary layer (SABL) (Parker et al. 2005; Stein et al. 2011; Bouniol et al. 2011; Roehring et al. 2013). The SMLC is the focus of this study.

The SMLC mostly consists of mixed-phase clouds that are non-precipitating but can affect the radiation budget, and hence can indirectly impact local precipitation by altering the environment for local small-scale convection or mesoscale convective systems entering the region. To understand how these clouds form, we need to understand the structure of the SABL. The SABL commonly reaches 5-6 km in height during summertime afternoon, and encompasses the Saharan convective boundary layer (SCBL) and the near-neutral Saharan residual layer (SRL) that caps it (Cuesta et al. 2009). From morning until early afternoon these two layers are separated by a weak temperature inversion (often 1K over 10-20 mb in height) caused by the previous day's fully developed SCBL (Messager et al. 2010; Garcia-Carreras et al. 2015). Furthermore, the strength and persistence of this inversion determines how well mixed the SCBL will be throughout the SABL, and ultimately the entrainment rate of free tropospheric air into the SABL. As the SCBL grows at the expense of the SRL, it reaches its full depth in late afternoon. The presence of such a weak capping inversion likely makes the representation of the evolution of the SABL by today's

climate models challenging, given that typical vertical grid-spacing are far greater than the thickness of the inversion.

Global atmospheric models fail to simulate accurately this mosaic of clouds associated with the African Monsoon and the Sahara desert. In particular, climate models severely underestimate the SMLC cover (Roehrig et al. 2013; Bourgeois et al. 2016). Underestimation of mid-level clouds in GCMs is not a problem only over the Sahara, but occurs globally (e.g., Zhang et al. 2005). The problem also exist in high resolution mesoscale research models such as the Weather Research and Forecast (WRF) atmospheric model (Cintineo et al. 2014; Thompson et al. 2016) and the German COSMO model (Eikenberg et al. 2016). This might be associated with the mixed-phase nature of these clouds (consisting of SLW and ice), and particularly with the underestimation of the SLW taking place in a thin layer in the upper part of the clouds (Barrett et al. 2016a; Barrett et al. 2016b). This thin layer of liquid water at cloud top has also been shown to dominate the radiative impact of these clouds (Hogan et al. 2003), by reflecting the shortwave radiation and consequently having a net cooling effect on the planet. Cloud feedbacks represent the largest source of uncertainty in future climate model predictions (Bony et al. 2006; Dufrense and Bony 2008; Andrews et al. 2012), and the generally poor simulation of mixed-phase clouds contributes to this uncertainty. It is also fair to assume that mesoscale numerical weather prediction (NWP) models as well as global models suffer from inadequate coverage of SLW and mixed-phase clouds partly due to model resolution, simply because model grid box average updrafts might be underestimating the sub-grid scale eddies and their vertical velocity that is required to produce the supersaturation to make clouds.

Another possible problem with GCMs or global NWP models is the representation of the surface characteristics, and for our case, the surface albedo over the Sahara desert. Modelling and theoretical studies show that horizontal heterogeneity of latent and sensible heating anomalies over the surface can induce local circulations that lead to convection (Froidevaux et al. 2018; Hohenegger and Stevens 2018). A similar mechanism may operate over the deserts having surface albedo variations.

The goal of this study is to simulate the Saharan mid-level clouds by running a regional atmospheric model over the study region at convection-permitting horizontal and vertical grid-spacing, which may allow a better simulation of convective and

cloud processes. Such an improvement will likely benefit the simulation of mid-level clouds in general in numerical weather prediction applications at operational centres that use more and more cloud-resolving and convection-permitting grid-spacing on global scales. The implications of our results for past climate, like the Green Sahara problem, are also discussed in section 4.

2. Data and methods

2.1 Observations

We use three sets of satellite observations for this study. First, we use 2006-2011 3-hourly precipitation rate derived from the Tropical Rainfall Measuring Mission (TRMM, product 3B42, Huffman et al. 2007). Second, we use 2006-2010 monthly mean 3-D cloud fraction from collocated CloudSat spaceborne radar (2B-GEOPROF version R04) CloudSat and Cloud-Aerosol Lidar (2B-GEOPROF-Lidar version R04) with Orthogonal Polarization (CALIOP; Kay and Gettelman 2009). These are sun-synchronous orbit satellites that are part of the A-train, and make roughly 32 equatorial overpasses at approximately 01:30 and 13:30 local time, which means that the observations over the Sahara are limited to this specific time of day. Third, we use 2005-2015 Top of the Atmosphere (TOA) Cloud Radiative Effect (CRE) for short wave, long wave and the net flux derived from Clouds and the Earth's Radiant Energy System (CERES) mission, edition 4.0. The CRE represent the difference between the observed radiative fluxes from broadband scanning radiometers on board Terra, Aqua and S-NPP satellites and the estimated clear-sky components.

2.2 Experimental design

The Weather Research and Forecast (WRF; Skamarok et al. 2008) atmospheric model is used to simulate the West African monsoon and conditions over the western Sahara. The experimental design is comprised of an outer domain D01 with 60 km horizontal grid-spacing, a nested intermediate domain D02 with 20 km grid-spacing,

and an inner nested domain D03 with 4 km grid-spacing (Figure 1a). The inner domain D03 covers the region of interest (20°W-14°E and 0°-32°N), i.e. the Sahel region, the western Sahara, and the surrounding ocean. Implementing a horizontal grid-spacing of 4 km enables us to deactivate the convective parameterization and explicitly represent deep convection. This does not mean that all convective processes, or even those that have a horizontal scale larger than 4 km, will be properly resolved; Skamarock (2004) showed the effective resolution of WRF in a configuration similar to our study is about seven times the grid spacing. Previous studies using models with similar numerics have shown that horizontal grid spacing of order 100m is needed to resolve individual deep convective drafts, while 4 km can adequately represent the overall storm structure and organizational mode (e.g., Bryan et al. 2003). The model uses ERA-*interim* reanalysis (Dee et al. 2011) as initial and lateral boundary conditions. All runs presented in the study cover the period July-September 2006. The choice of the year was made given that it is the first year where 3-D cloud fraction is available from the satellite data.

All simulations are run with 1-way nesting. Our simulations use the Betts-Miller-Janjic convective scheme for the outer domains, the Mellor-Yamada-Janjic planetary boundary layer scheme for all domains, and the two-moment Morrison scheme (Morrison et al. 2009) for the microphysics.

Also, given observations of tropical *altocumulus* with a variety of instruments by Ansmann et al. (2009), who found that almost all of the cloud layers had SLW at the top down to -35°C, the nucleation of ice by deposition and condensation freezing in the scheme was modified to only occur at temperatures below this value (compared to the default value of -8°C). This has the effect of increasing the amount and lifetime of SLW in mid-level cloud layers, since this limits the depletion of supercooled droplets by ice crystals. Note that ice can still form at temperatures above −35°C from heterogeneous freezing of pre-existing supercooled cloud droplets and rain. Additionally, we use a cloud-fraction scheme (option *icloud*=3) that uses a critical relative-humidity threshold (that is grid-spacing dependent) for the onset of non-zero cloud amount, along with a cloud fraction that increases with RH following Sundqvist et al. (1974). This option was created to improve a generally known deficiency of low and mid-level clouds, consistent with previous studies (e.g., Cintineo et al. 2014; Eikenberg et al. 2015; Thompson et al. 2016) and initially appears to create better

total cloud forecasts through comparisons with solar radiation observations in North America (Thompson et al. 2016).

Initially, the model is run with a vertical grid (38 levels, Fig 1, Supplementary material) that is close to what GCMs typically use, but later we present results using higher vertical resolution (see below). Our simulations also test the sensitivity of atmospheric conditions over the Sahara to the surface albedo. For this, first we use a simple surface albedo scheme, which is constant with time and is based on vegetation types (Figure 1c), before using a more realistic time-varying surface albedo (Figure 1d) that is derived from the MODIS satellite dataset (Schaaf and Wang, 2015). This albedo has a resolution of 1 km, but is interpolated to the 4 km grid spacing of the WRF inner domain.

3. Results

All simulations produce strong rainfall in the tropical regions and scattered mid-level cloud systems over the Sahara. Many of the mid-level clouds over the Western Sahara (10°W-10°E) are advected into the region by a clockwise circulation associated with the mid tropospheric Saharan high (centred at 25°N) located above the lower tropospheric Saharan low, as reported by Chen (2005). On occasions, clouds also appear to result from detrainment from cumulus clouds from the south, seen as northward bursts of tropical convection from the monsoon region. For an animated view of these and other qualitative features, the reader is referred to a video available in the Supplementary Information.

Compared with observations (Figure 2a), our baseline simulation captures, at least in the zonal mean sense, the July-September (JAS) cloud amount distribution reasonably well in the monsoon region (Figure 2b). It captures the position of the low stratocumulus clouds over the Gulf of Guinea, as well as the deep convective clouds associated with the African monsoon (5-17°N) except that the upper troposphere cloud fraction is overestimated by roughly 50%. The last is associated with a well-known bias of the Morrison 2-moment microphysical scheme that produces excessive upper level low temperature clouds (Cintineo et al. 2014).

Our simulation also captures the position of the Saharan mid-level cloud layer, but severely underestimates the cloud amount in that layer with maximum values from 2 to 4% between 20-30°N, which is small compared to the observed ~24% (Figure 2a). Given the limited daily sampling of the satellite data, we also show the zonal mean JAS cloud fraction averaged from 2006 to 2010 (Figure 2, supplementary material), where the mid-level Saharan cloud fraction appears slightly reduced, with a maximum ~20%.

3.1 Role of vertical resolution

One possible explanation for the shortfall of simulated clouds is that the limited vertical resolution (38 levels), with a maximum of 4-5 levels at heights typical of mid-tropospheric cloud layers over the Sahara, is unable to capture the structure of these clouds. To test this idea we conduct a similar run but with increased vertical resolution, 87 levels (hereafter 87Lev), with roughly 18 levels within the Saharan mid-level cloud layer. The resulting zonal mean cloud fraction is significantly improved over the Sahara between 20-30°N, with maximum daily mean cloud fraction from 5 to 8% (Figure 2c), still smaller compared to the observed 24% (Figure 2a). This difference between the simulated and the observed cloud fraction may be partly explained by the fact that the cloud profiling radar on board CloudSat is unable to distinguish clouds from elevated precipitation and snow, leading in some cases to observed precipitation being interpreted as clouds (Mace et al. 2009). The same argument can be used to explain the occasional presence of observed clouds within the first 4000 meters of the atmosphere, as opposed to the simulated lower atmosphere that appears to be cloud free. Roehrig et al. (2013), after using the same satellite dataset, found a smaller observed zonal mean cloud fraction and no clouds between 0-4000 meters after discarding the precipitating water phase from the satellite observations.

A third simulation with even higher vertical resolution (109 levels, hereafter 109Lev), with 27 levels within the Saharan mid-level cloud layer, did produce slightly more Saharan mid-level clouds in the zonal mean between 20-30°N, with maximum values from 6 to 9% (not shown). It should be noted that the grid spacing for the

109Lev is only slightly denser compared to 87Lev, which also probably explains why the increase in clouds is not that impressive. Despite this, and despite that the mid-level Saharan clouds are still underrepresented, our experiments show that vertical grid-spacing plays a crucial role, with more levels increasing the model's ability to simulate these clouds. The question is why?

First of all, there is the physical aspect. These clouds are relatively thin; thickness varies from 100-200 meters to 3-4 km, much thinner than the deep convective clouds farther south. A model with a coarse vertical grid-spacing within the mid-level cloud zone (between 600 and 400 hPa) will struggle to simulate thinner layers of high relative humidity, and consequently the resulting clouds or their effects on the surface energy budget. Furthermore, mid-level clouds exhibit constant rising and sinking motion throughout the cloud layer, which is driven by long-wave radiation cooling at cloud-top. This means that coarse vertical resolution simulations won't be able to resolve properly the overturning dynamics that help maintained these clouds.

Second there are also microphysical reasons that have to do with the interaction of liquid water and ice within the clouds. To explain this, we compute the ratio:

$$\left\langle \frac{q_{liq}}{q_{ice} + q_{liq}} \right\rangle$$

where, q_{liq} and q_{ice} represent the mixing ratios of liquid water and ice, and the brackets represent the zonal, meridional, daily and seasonal average (Figure 3). The liquid plus ice mixing ratio was chosen for the denominator as opposed to ice mixing ratio in order to avoid giving increased weight to clouds with very small ice concentration. The ratio varies from 0 to 1, and profiles show the lack of ice in the lower levels, and the lack of liquid water in the upper levels of the troposphere, respectively. The most important finding here is that the more vertical levels we use the more we increase the ratio in the upper part of the clouds, which means that the amount of SLW relative to the amount of ice increases. The presence of SLW at the top of mid-level clouds has been observed previously all over the globe, i.e. the Arctic, the mid-latitudes, the Southern Ocean, the tropics and the Sahara during the summer season (Zhang et al. 2010), but climate models often severely underestimate the amount observed (Barrett et al. 2017a). This is partly because coarse vertical resolution, by definition, is unable to represent thin mid-level supercooled liquid layers. In our case, the increased fraction of the total condensate that is taken by ice in

a configuration with a limited number of vertical levels (Lev38) means that, once liquid water and ice are mixed at a certain model level, all the liquid water goes to ice. This is because the vapour saturation pressure over ice is always smaller than that over liquid water at a given temperature (Bergeron-Wegener-Findeisen process). Eventually the ice will fall out of the cloud, resulting in clouds with a short lifetime. In contrast, more vertical levels allow layers of ice and liquid water to exist separately; clouds are not depleted of liquid water so rapidly, allowing the clouds a longer lifetime. This is consistent with the findings of Barrett et al. (2017b) who has shown that coarse vertical grid spacing (500 m) models are unable to simulate the thin and long-lived supercooled liquid layer at the top of mid-level clouds, and only when a much finer grid spacing (50-100 m) is implemented the amount and lifetime of the supercooled liquid layer is properly simulated.

Third, a heating feedback may amplify changes in cloud amount due to the above factors. Table 1 outlines the mean surface energy budget terms (averaged from 10°W to 10°E, and 23 and 27°N) for the time of day when the clouds reach maximum (19:00-20:00 UTC) and minimum (11:00-12:00 UTC) amounts (see bellow). During the day, these mid-level clouds have on average a net cooling effect (with the exception of the very thin ones that have a warming effect) of up to a few degrees. This can also be seen by the decrease in the positive net surface heat flux (by 3.8 $W \cdot m^{-2}$) as cloudiness increases with higher vertical resolution, signifying less surface warming. This is because the reduction in the net surface SW radiation cannot be balanced by the increase in the net LW radiation or the reduction in the heat flux leaving the ground through sensible and latent heating.

On the other hand, during the evening and night hours these clouds have a warming effect, which can be seen by the increase in the negative net surface heat flux by 2 $W \cdot m^{-2}$ (Table 2) as cloudiness increases with higher vertical resolution, signifying less surface cooling. This is the result of the greenhouse effect of the clouds by increasing the net surface LW radiation. The result is that, during the evening and night hours, areas covered by clouds appear several degrees warmer on average compared to the cloud free surrounding environment, with the warming effect increasing as the clouds become deeper (not shown). The increased upwelling LW flux associated with the warmer surface and subsequent cloud base warming could help to sustain convective mixing in mid-level altocumulus layers during night time,

when the cloud layer and the surface become decoupled. This could play a role in helping to maintain the cloud layer through a positive feedback on cloud formation. This idea is supported by a PDF of the vertical velocity over the Sahara (Figure 4) confirming that when the model vertical resolution increases, the upward and downward motions in the mid-troposphere intensify, indicating a more vigorous mid-level cloud overturning. Such evidence suggests that once these clouds are formed they may become self-sustained during the evening and night hours. Note that analysis of the zonal-mean vertical velocity does not show any systemic change in the large scale overturning circulation over the Sahara with higher vertical resolution (not shown).

3.2 Role of surface albedo heterogeneity

Another possible influence on clouds is the specification of the surface albedo. Surface albedo is an important geophysical property of land surfaces that represents the fraction of incoming solar radiation reflected back to the atmosphere. Also, over the desert, where there is little vegetation and soil moisture, it is the only geophysical property that affects the surface energy budget. So far, our simulations use surface albedo that is derived from globally defined vegetation categories and is spatially uniform over the Sahara (0.38). However, this is not very realistic (Cuesta et al. 2009; Kealy et al. 2017), since the Saharan desert albedo varies spatially throughout from 0.14 to 0.51, with sharp horizontal gradients (Figure 1d).

Therefore, we conduct an additional simulation, which implements the MODIS albedo (87LevM), but otherwise is similar to 87Lev. This configuration was chosen over the 109Lev due to the high computational cost of the latter. Although the mean surface albedo over the Sahara (averaged from 10°E-10°W, 20-30°N) is not very different between the 87Lev and 87LevM runs (0.378 and 0.340, respectively), the latter exhibits a zonal-mean cloud fraction that is considerably increased between 20-30°N, with maximum values from 7 to 11% (Figure 2d) compared to 5-8% in 87Lev. Thus we conclude that both vertical resolution and surface albedo matter for the simulation of the Saharan mid-level clouds and therefore should be represented adequately in models.

Regarding the mechanism of the increase in cloud fraction for 87LevM, the vertical profile of the water-to-ice mixing ratio in the middle part of the Saharan cloud layer (5.5-7 km) is not increased compared to 87Lev, which indicates that the increase in cloud fraction is not achieved through microphysics. The difference in cloud fraction is in this case associated with a change in the spatial distribution of the mid-level clouds over the Sahara (Figure 5). 87LevM exhibits a cloud distribution that resembles that of the surface albedo, with increased cloudiness over areas with lower albedo. A histogram (Figure 6) reveals that over the desert (20-30°N) the vertically averaged cloud fraction is a quasi-linear function of the surface albedo during evening hours, when mid-level clouds are most abundant (shown below). In contrast, during midday, when mid-level clouds are at their weakest, surface albedo has almost no effect on cloud formation. This relationship also reveals that areas with albedo larger than 0.5 experience throughout the day cloudiness that approaches zero.

This is consistent with the idea that areas of lower albedo experience a larger warming, affecting the horizontal temperature and pressure gradients between areas of high and low albedo, thus leading to more convection over the latter. Such local maxima in mid-level cloud formation, which have been attributed to the surface albedo contrast, have been previously reported in observations (Cuesta et al. 2009; Kealy et al. 2017). In contrast, in 87Lev clouds are distributed rather spatially uniformly. This simulation does however show that in some cases, elevated terrain slightly favours mid-level cloud formation, even if surface albedo is spatially homogenous. This can be seen west of the Hoggar mountains (2900 meters high, 6°E-24°N), as well as elevated terrain to the south-west (3°E-20°N).

Our simulations also capture the diurnal cycle of the SMLCs. Previously, the diurnal cycle of the SMLC has been investigated using satellite data provided by CloudSat and CALIPSO, launched in 2006 (Stein et al. 2011). Figure 7 shows that, regardless of vertical resolution, the mid-level clouds over the Sahara exhibit a diurnal behaviour that resembles a simple sinusoidal wave. They are more frequent during nightime (maximum frequency at 20-21:00 UTC) and less during daytime, which we know from observations is quite common for mid-level clouds in general (Bouniol et al. 2011, Stein et al. 2011; Riihimaki et al. 2012).

However, comparing cloud fraction derived from satellite data with cloud fraction from model output could raise some concern, since a “cloud” in the mode is

not the same as a cloud detected by satellite retrievals. We therefore compare the simulated Cloud Radiative Effect (CRE) with CERES observations (Table 3) averaging between (10°W-10°E and 25-29°N) to include only the effect of the mid-level clouds and avoid high and convective clouds to the south, which our simulations tend to overestimate. In the observations the LW component of the CRE dominates over the SW component, resulting in a net warming effect of 7-8 W/m2. Comparing the CRE from 2006 with that of 2005-2015 climatology reveals that year 2006 was a normal year in terms of cloud amount. In our model simulations, CRE_{SW} and CRE_{LW} both increase with cloud amount as resolution increases, with the 87LevM run the most accurate. It captures very well the SW cooling effect (-8 Wm^{-2}), but underestimates the LW warming effect by roughly 5 Wm^{-2}.

The CRE_{LW} disagreement can be attributed to a number of factors. First, satellite derived CRE_{LW} tend to overestimate the actual value, because the atmosphere has more water vapour when it is cloudy, and the clear-sky CRE_{LW} monthly value is obtained only from days with no clouds and a dryer atmosphere (Sohn and Bennartz 2008). In contrast, model derived clear-sky OLR is obtained at all times but with the clouds left out of the radiation calculation, resulting in smaller clear-sky OLR, and consequently smaller CRE_{LW} compared to that from satellites. Sohn et al. (2006) found that over the Sahara, satellite derived CRE_{LW} is overestimated due to upper tropospheric humidity associated with the presence of clouds by 4-7 Wm^{-2}, which is already enough to explain our 5 Wm^{-2} discrepancy. Another possible explanation would be if the model underestimates the cloud fraction, but at the same time overestimates cloud opacity. In this case the CRE_{SW} could by accident come out correct while the CRE_{LW}, which is insensitive to cloud opacity, would come out too small. Overall, the CRE from 87LevM and CERES data agree with each other suggesting that our model captures a good portion of the observed cloud amount or at least its radiative effect.

Regarding the zonal-mean precipitation, despite the model's dry bias south of 10°S in all simulations (possibly the result of biases in the SSTs used to force the model), north of 10°N it is simulated reasonably well compared to the TRMM satellite data (Figure 8). When the simple albedo is used, the simulated precipitation falls to zero much too abruptly around 15°N and over the desert, north of 17°N, rain is significantly underestimated. These characteristics are shared among all three

simulations that use the simple surface albedo. However, when the MODIS albedo is used instead in Lev87M, the simulated zonal precipitation profile well matches that of TRMM on the northern portion of the monsoon, and the dry bias between 17-25°N is significantly reduced, which shows the importance of representing the surface characteristics accurately. Additionally, horizontal surface albedo heterogeneities also seem to impact the horizontal distribution of precipitation on the northern edge of the monsoon (16-21°N), where the climate transitions from a wet to a desiccated one. Figure 9 shows that seasonal precipitation is a quasi linear function of surface albedo, with low albedo anomalies favouring 2-4 times more precipitation than the high albedo ones. It also shows that this linear relation becomes weaker (slope gets smaller) as we move north, and north of 22°N the albedo seems to have no effect on seasonal mean precipitation. A similar relationship can be found south of 16°N with greater precipitation rates (not shown), but the surface albedo range is much smaller given the extensive vegetation cover in the monsoon region.

The above results are in agreement with recent studies showing that surface heterogeneities caused by tropical deforestation (Souza et al. 2000) or idealized bipolar sensible and latent heating anomalies (Froidevaux et al. 2018; Hohenegger and Stevens 2018) play a crucial role in organizing local convection. In analogy, our result show that heating anomalies caused by anomalies of surface albedo are equally important, for the creation of clouds and precipitation, even in a desiccated environment like the Sahara desert.

4. Implications for Mid-Holocene Sahara Greening

The accurate simulation of the SMLCs is important for past climate as well. A variety of paleo-proxy data suggest that during the Mid-Holocene (6000 years ago), the southern Sahara desert was considerably smaller compared to present day, with step vegetation and large lakes penetrating further north (Kusnir and Moutaye, 1997; Jolly et al. 1998; Ghienne et al., 2002; Schuster et al., 2003, 2005, 2009; Drake and Bristow, 2006; Leblanc et al., 2006; Wu et al. 2007; Bouchette et al., 2010; Lezine et al. 2011). Such evidence suggests that during the Mid-Holocene the Sahara desert experienced considerably more precipitation compared to present day conditions due

to a periodic change in Earth's orbit. In general the Mid-Holocene was associated with stronger monsoons due to an orbitally induced strengthening of the insolation contrast between summer and winter season (Joussaume et al. 1999; Mantsis et al. 2013).

Modelling studies have shown that a number of local and remote feedbacks may have contributed to the greener Mid-Holocene Sahara: a) vegetation-albedo feedback (Kutzbach et al. 1998), dust feedback (Pausata et al. 2016), c) "Mega Lakes" feedback, d) SST feedback (Su and Neelin 2005), and Eurasian vegetation feedback (Swann et al. 2014). The above feedbacks are all positive, but taking them into account still fails to produce simulations of Mid-Holocene precipitation anomalies that are large enough to support the vegetation suggested by the proxies or the existence of a Mega-Chad lake (Harrison et al. 2015).

There are two possible reasons for this. First, the Mid-Holocene Sahara Greening has been studied using low resolution GCMs that represent convection with uncertain parameterizations that severely underestimate the Saharan Mid-Holocene clouds and their radiative impact for today's climate. A high-resolution model that captures the correct mid-level cloud amount over the Sahel/Sahara as well as its radiative impact is likely to capture the climate response to a change in the TOA insolation more accurately.

Second, GCMs predict that all known feedbacks associated with the Mid-Holocene are positive. However, the opposite cannot be ruled out. For example, Hohenegger et al. (2009) has shown that positive soil moisture anomalies have a negative feedback on the summer precipitation in Central Europe when using 2 km horizontal resolutions (convection permitting), but a positive feedback when using 25 km horizontal resolutions (convection is parameterized). A similar case should not be ruled out in the Green Sahara problem, since a greener Sahara is associated with more vegetation and more soil moisture. Of course, a greener Sahara would also be associated with a different albedo that would further change the surface energy budget. We suggest that a regional model operating at convection permitting horizontal and vertical grid-spacing that captures both clouds and feedbacks might be able to address a problem like the Mid-Holocene Sahara Greening that has challenged low-resolution GCMs. Future plans include simulations that address this topic with a high resolution regional model, that will also include the feedbacks associated with the Mid-Holocene.

5. *Discussion*

GCMs have failed to simulate accurately Saharan mid-level clouds (Roehrig et al. 2013). Our study shows that the use of cloud- and convection-permitting grid spacing (4 km) produces a good diurnal cycle of clouds, but is not enough to simulate properly the amount of Saharan clouds. It is only when the vertical resolution becomes high enough to allow layers of liquid water and layers of ice to exist separately that simulated clouds start to approach realistic amounts. Today's GCMs used for climate studies have only a limited number of vertical levels (roughly 30), with a maximum of 4-5 levels at heights typical of mid-tropospheric cloud layers over the Sahara, which can stretch 3-4 km in the vertical. Our results suggest that such a configuration will limit these models' ability to simulate the full spectrum of clouds over the Sahara. We find that the use of grid spacing on the order of 100-200 meters allows the simulation of a Saharan mid-level cloud layer, but still it underrepresents the observed cloud amount, suggesting that an even higher vertical grid-spacing (50 m) should be used. One possible configuration, that future studies of Sahara mid-level clouds could implement, in order to maintain computational efficiency, is to use a dense vertical resolution between 4-8 km, but keep a coarser grid-spacing above and below this layer. The same arguments could also be used for improving the simulation of mid-level clouds in general in numerical weather prediction applications, which use more and more often cloud-resolving or convection permitting grid-spacing.

Increasing the vertical resolution may seem a straightforward way to fix the problem, but it does have limitations. First of all, implementing a very dense vertical grid-spacing will result in high computational cost and computational efficiency. Besides this, it is also likely that at some point the effect will saturate, where adding more vertical levels will not result in better cloud simulation. We were not able to obtain a full satisfactory simulation of mid-level clouds by high resolution alone. While our study tested only the Morrison 2-moment microphysical scheme, it is reasonable to expect that models with other microphysical schemes might also improve as vertical resolution increases.

An additional simulation using high-resolution, satellite-derived surface albedo shows that it is also necessary to represent accurately surface conditions to simulate Saharan clouds correctly. Using the MODIS albedo resulted roughly in a 30%

increase in the zonal mean cloud fraction compared to a similar simulation that used a surface albedo that was uniform over the desert but with nearly the same zonal mean.

Some limitations do apply to our study. Given the high computational cost of running the WRF model at this horizontal and vertical grid-spacing, our simulations cover only one season (July-September 2006), which poses some challenges. Also, satellite data are much coarser in space and time compared to the model output, with sampling taking place only twice a day. Additionally, the effective resolution of any Eulerian numerical simulation is several times the grid spacing, which means that processes spanning only a few model grids are only marginally represented. In an aircraft-based study, Kealy et al. (2017) reported that 67% of the clouds encountered have a horizontal scale smaller than 3 km, and that the most frequently observed (25%) were also the smallest cloud size identifiable by the aircraft instrumentation (300m). A higher horizontal resolution might allow the model to simulate the thinner and smaller altocumulus clouds that are absent from our simulations.

These limitations are crucial because it may limit the model ability to accurately simulate the precipitation over the Sahara during past climate. Also, it could compromise the models ability to estimate the net mid-tropospheric heating of the Saharan clouds and any remote effect this might have on the global circulation. Given that the CRE_{NET} of these clouds is at least twice as that of the green-house gas radiative forcing, such a bias might prove crucial for future climate projections. Therefore, future studies addressing these topics, would have to implement a finer convection permitting horizontal and vertical grid-spacing along with covering multiple seasons to address the role of the mid-level Saharan cloud layer more completely for regional or global climate.

Acknowledgements: This work is funded by a Laureate Fellowship (FL150100035) from the Australian Research Council. The computations were carried out with high performance computing support provided by the National Computing Infrastructure (NCI) in Canberra, Australia. The data produced for and analysed in this paper are archived at NCI and can be provided upon request. We would also like to thank Kartin Meissner for her useful comments.

References

Andrews, T., J. M. Gregory, M. J. Webb, and K. E. Taylor (2012): Forcing, feedbacks and climate sensitivity in CMIP5 coupled atmosphere-ocean climate models. *Geophys. Res. Lett.*, *39*, L09712, doi:10.1029/2012GL051607.

Ansmann, A., and Coauthors, 2009: Evolution of the ice phase in tropical altocumulus: SAMUM lidar observations over the Cape Verde. *J. Geophys. Res.*, D17208, doi:10.1029/2008JD011659.

Barrett, A. I., R. J. Hogan, and R. M. Forbes, 2017a: Why are mixed-phase altocumulus clouds poorly predicted by large-scale models? Part 1. Physical processes. *J. Geophys. Res.*, doi: 10.1002/2016JD026321.

Barrett, A. I., R. J. Hogan, and R. M. Forbes, 2017b: Why are mixed-phase altocumulus clouds poorly predicted by large-scale models? Part 2. Vertical resolution sensitivity and parameterization. *J. Geophys. Res.*, doi: 10.1002/2016JD026322.

Bony, S., et al. (2006): How well do we understand and evaluate climate change feedback processes? *J. Clim.*, ***19***, 3445–3482.

Bouchette, F., and Coauthors, 2010: Hydrodynamics in Holocene lake Mega-Chad. *Quaternary Res.*, **73**, 226-236.

Bouniol, D., and Coauthors, 2011: Diurnal and seasonal cycles of cloud occurrences, types, and radiative impact over west Africa. *J. App. Meteo. Clim.*, **51**, 534-552.

Bourgeois, Q., A. M. L. Ekman, M. R. Igel, and R. Krejci, 2016: Ubiquity and impact of thin mid-level clouds in the tropics. *Nature com.*, 7:12432, doi:10.1038.

Bryan, G. H., J. C. Wyngaard, and J. M. Fritsch, 2003: Resolution requirements for the simulation of deep moist convection. *Mon. Wea. Rev.*, **131**, 2394-2416.

Chen, T.-C., 2005: Maintenance of the midtropospheric North African summer circulation Saharan high and African easterly jet. *J. Clim.*, **18**, 2943-2962.

Cintineo, R., Otkin, J.A., Xue, M., Kong, F., 2014. Evaluating the performance of planetary boundary layer and cloud microphysical parameterization schemes in convection- permitting ensemble forecasts using synthetic GOES-13 satellite observations. Mon. Weather Rev. 142, 163–182.

Cuesta, J., J. H. Marsham, D. J. Parker, and Cyrille Flamant, 2009: Dynamical mechanisms controlling the vertical redistribution of dust and the

thermodynamic structure of the West Saharan atmospheric boundary layer during summer. *Atmos. Sci. Let.*, doi: 10.1002/asl.207.

Dee, D. P., and Coauthors, 2011: The ERA-Interim reanalysis: configuration and performance of the data assimilation system. *Q. J. R. Meteorol. Soc.*, **137**, 553-597, doi:10.1002/qj.828.

Drake, N., and C. Bristow, 2006: Shorelines in the Sahara: geomorphological evidence for an enhanced Monsoon from palaeolake Megachad. *Holocene*, **16**, 901-911.

Dufresne, J. L., and S. Bony (2008): An assessment of the primary sources of spread of global warming estimates from coupled atmosphere-ocean models. *J. Clim.*, **21**, 5135–5144.

Eikenberg, S., C. Kohler, A. Seifert, S. Crewell, 2015: How microphysical choices affect simulated infrared brightness temperatures. *Atmos. Res.*, **156**, 67-79.

Froidevaux P., L. Schlemmer, J. Schmidli, W. Langhans, and C. Schar, (2014): Influence of the background wind on the local soil moisture-precipitation feedback. *J. Atmos. Sci.*,**71** ,782–799.

Garcia-Carreras, L., and Coauthors, 2015: The turbulent structure and diurnal growth of the Saharan atmospheric boundary layer. *J. Atmos. Sci.*, **72**, 693-713.

Ghienne, J. F., M. Schuster, A. Bernard, P. Duringer, and M. Brunet, 2002: The Holocene giant lake revealed by digital elevation models. *Quaternary Int.*, **87**, 81-85.

Harrison, S. P., P. J. Bartlein, K. Izumi, G. Li, J. Annan, J. Hargreaves, P. Braconnot, and M. Kageyama, 2015: Evaluation of CMIP5 paleo-simulations to improve climate projections. *Nature Climate Change*, **5**, 735-743.

Hogan, R. J., P. N. Francis, H. Flentje, A. J. Illingworth, M. Quante, and J. Pelon, 2003: Characteristics of mixed-phase clouds: Part I: Lidar, radar, and aircraft observations from CLARE'98. *Q. J. R. Meteorol. Soc.*, **129**, 2089-2116.

Hohenegger, C., P. Brockhaus, C. S. Bretherton, and C. Schar, 2009: The soil moisture-precipitation feedback in simulations with explicit and parameterized convection. *J. Clim.*, **22**, 5003-5020.

Hohenegger, C., and B. Stevens, 2018: The role of the permanent wilting point in controlling the spatial distribution of precipitation. *PNAS*.

Huffman, G. J., D. T. Bolvin, E. J. Nelkin, D. B. Wolff, R. F. Adler, G. Gu, Y. Hong, K. P. Bowman, and E. F. Stocker, 2007: The TRMM Multisatellite Precipitation Estimates at Fine Scales. *J. Hydrometeorol.*, **8** (1), 38-55.

Jolly, D., and Coauthors, 1998: Biome reconstructions from pollen and plant macrofossil data for Africa and the Arabian Peninsula at 0 and 6 ka. *J. Biogeogr.*, **25**, 1007-1027.

Joussaume, S., and Coauthors, 1999: Monsoon changes for 6000 years ago: Results of 18 simulations from the Paleoclimate Modeling Intercomparison Project (PMIP). *Geophy. Res. Lett.*, **26**, 859-862.

Kay, J. E., and A. Gettelman, 2009: Cloud influence on and response to seasonal Arctic sea ice loss. *J. Geophys. Sci.*, **114**, D18204.

Kealy, J. C., and Coauthors, 2017: Clouds over the summertime Sahara: an evaluation of Met Office retrievals from Meteosat Second Generation using the airborne remote sensing. *Atmos. Chem. Phys.*, **17**, 5789-5807.

Knippertz, P., A. H. Fink, R. Schuster, J. Trentmann, J. M. Schrage, and C. Yorke, 2011: Ultra-low clouds over the southern West Africa monsoon region. *Geophys. Res. Lett.*, **38**, L21808.

Kusnir, I., and H. A. Moutaye, 1997: Ressources minerals du Tchad: une revue. *J. Afr. Earth Sci.*, **24**, 549-562.

Kutzbach, J., G. Bonan, J. Foley, and S. P. Harrison, 1998: Vegetation and soil feedbacks on the response of the African monsoon to orbital forcing in the early to middle Holocene. *Nature*, **384**, 423-426.

Leblanc, M., and Coauthors, 2006: Reconstruction of Megalake Chad using Shuttle Radar Topographic Mission data. *Paaleogeogr. Palaeocl.*, **239**, 16-27.

Lezine, A.-M., W. Zheng, P. Braconnot, and G. Krinner, 2011: Late Holocene plant and climate evolution at Lake Yoa, northern Chad: Pollen data and climate simulations. *Climate Past*, **7**, 1351-1362.

Mace, G. G., and Coauthors, 2009: A description of hydrometeor layer occurrence statistics derived from the first year of merged Cloudsat and CALIPSO data. *J. Geophys. Res.*, **114**, D00A26.

Mantsis, D. F., A. Clement, B. Kirtman, A. J. Broccoli, and M. P. Erb, 2013: Precessional cycles and their influence on the North Pacific and North Atlantic summer anticyclones. *J. Clim.*, **26**, 4596-4611.

Messager, C., D. Parker, O. Reitebuch, A. Agusti-Panareda, C. M. Taylor, and J. Cuesta, 2010: Structure and dynamics of the Saharan atmospheric boundary layer during the West African monsoon onset: Observations and analysis from the research flights of 14 and 17 July 2006. *Quart. J. Roy. Meteo. Soc.*, **136**, 107-124.

Morrison, H., G. Thompson, and V. Tatarskii, 2009: Impact of cloud microphysics on the development of trailing stratiform precipitation in a simulated squall line: Comparison of one- and two-moment schemes. *J. Clim.*, **137**, 991-1007.

Parker, D. J., C. D. Thorncroft, R. R. Burton, and A. Diongue-Niang, 2005: Analysis of the African easterly jet, using aircraft observations from the JET2000 experiment. *Q. J. R. Meteorol. Soc.*, **131**, pp 1461-1482.

Riihimaki, L. D., McFarlane S. A., Comstock J. M., 2012: Climatology and formation tropical of mid-level clouds at the Darwin ARM site. *J. Clim.*, **25**, 6835-6850.

Roehrig, R., D. Bouniol, F. Guichard, F. Hourdin, J.-L., Redelsperger, 2013: The present and future of the West African monsoon: A process-orientated assessment of CMIP5 simulations along the AMMA transect. *J. Climate*, **26**, 6471-6505.

Pausata, F. S. R., G. Messori, and Q. Zhang, 2016: Impact of dust reduction on the northward expansion of the African monsoon during the Green Sahara period. *Earth and Planerary Sci. Lett.*, **434**, 298-307.

Schaaf, C., and Z. Wang, 2015: MCD43A3 MODIS/Terra+Aqua BRDF/Albedo Daily L3 Global – 500m V006. NASA EOSDIS Land Processes DAAC. doi: 10.5067/MODIS/MCD43A3.006.

Schuster, M., P. Duringer, J. F. Ghienne, M. Brunet, and P. Vignaud, 2003: Coastal conglomerates around the Hadjer el Khamis inselbergs (Chad): new evidence for Lake Mega-Chad high water level episodes. *Earth Surf. Proc. Land.*, **28**, 1059-1069.

Schuster, M., and Coauthors, 2005: Holocene Lake mega-Chad palaeoshorelines from space. *Quaternary Sci. Rev.*, **24**, 1821-1827.

Scuster, M., and Coauthors, 2009: Chad Basin: paleoenvironments of the Sahara since the Late Miocene. *C. R. Geosci.*, **341**, 603-611.

Skamarock, W. C., 2004: Evaluating mesoscale NWP models using kinetic energy spectra. *Mon. Wea. Rev.*, **132**, 3019-3032.

Skamarock, W. C., and Coauthors 2008: A description of the advanced research WRF version 3. NCAR Tech. Note NCAR /TN-475+STR.

Sohn, B.-J., 2006: Dry bias in satellite-derived clear-sky water vapour and its contribution to longwave cloud radiative forcing. *J. Clim.*, **19**, 5570-5580.

Sohn, B.-J., and R. Bennartz, 2008: Contribution of water vapour to observational estimates of longwave cloud radiative forcing. *J. Geophys. Res. Atmos.*, **113**, DOI: 10.1029/2008JD010053.

Souza, E. P., N. O. Renno, and M. A. F. Silva Diaz, 2000: Convective circulations induced by surface heterogeneities. *J. Atmos. Sci.*, **57**, 2915-2922.

Stein, T. H., and coauthors, 2011: The vertical cloud structure of the West African monsoon: A 4 year climatology using CloudSat and CALIPSO. *J. Geophys. Res.*, **116**, D22205.

Su, H., and D. J. Neelin, 2005: Dynamical mechanisms for African monsoon changes during the mid-Holocene. *J. Geophys. Res.*, **110**, D19105.

Sundqvist, H., E. Berge, and J. E. Kristjansson, 1989: Condensation and cloud parameterization studies with a mesoscale numerical weather prediction model. *Mon. Weather Rev.*, 117, 1641–1657.

Swann, A. L., I. Y. Fung, Y. Liu, and J. C. H. Chiang, 2014: Remote vegetation feedbacks and the Mid-Holocene green Sahara. *J. Climate*, **27**, 4857-4870.

Thompson, G., M. Xu, and P. Jimenez, 2016: Towards improving cloud representation in WRF using a cloud fraction scheme. *FAA Task Report*, Aug 2016.

Wu, H., J. Guiot, S. Brewer, and Z. Guo, 2007: Climate changes in Eurasia and Africa at the last Glacial maximum and mid-Holocene: Reconstraction from pollen data using inverse vegetation modeling. *Climate Dyn.*, **29**, 211-229.

Zhang, M. H., and Coauthors, 2005: Comparing clouds and their seasonal variations in 10 atmospheric general circulation models with satellite measurements. *J. Geophys. Res.*, **110**, D15S02, doi:10.1029/2004JD005021.

Zhang, D., Z. Wang, and D. Liu, 2010: A global view of midlevel liquid-layer topped stratiform cloud distribution and phase partition from CALIPSO and CloudSat measurement. *J. Geophys. Res.*, doi: 10.1029/2009JD012143.

Tables

Table 1. Partitioning of the surface energy budget (W/m^2) for August 2006, averaged for 11-13:00 UTC. Positive (negative) sensible or latent heat flux means heat going out of (into) the ground.

	SW↓	SW↑	LW↓	LW↑	SH	LH	Q_{NET}
38 lev	921.8	301.4	399.0	556.6	288.9	79.8	94.1
87 lev	887.6	292.4	402.3	555.5	276.1	75.7	90.3
109 lev	880.9	290.6	403.6	555.3	272.9	75.9	89.8

Table 2. Same as Table 1, but for 20-22:00 UTC.

	SW↓	SW↑	LW↓	LW↑	SH	LH	Q_{NET}
38 lev	-	-	388.9	456.7	-16.2	7.1	-58.7
87 lev	-	-	395.3	460.6	-15.8	7.0	-56.5
109 lev	-	-	396.7	460.4	-15.0	7.3	-56.0

Table 3. Average Cloud Radiative Forcing (CRF), defined as the difference between the TOA clear-sky radiation terms and the real counterparts for the WRF simulation and CERES satellite retrievals. The first are hypothetical quantities and are computed by the radiation scheme assuming zero cloudiness. CRE has been averaged between (10°W-10°E and 25-29°N), and covers the July-September period.

	38Lev (2006)	87Lev (2006)	87LevM (2006)	109Lev (2006)	CERES (2006)	CERES (2005-2015 clim.)
LW	6.5	10.1	11.1	9.8	16.5	15.7
SW	-3.4	-6.0	-8.0	-6.0	-8.7	-8.5
NET	3.1	4.2	3.1	3.8	7.8	7.2

Figures

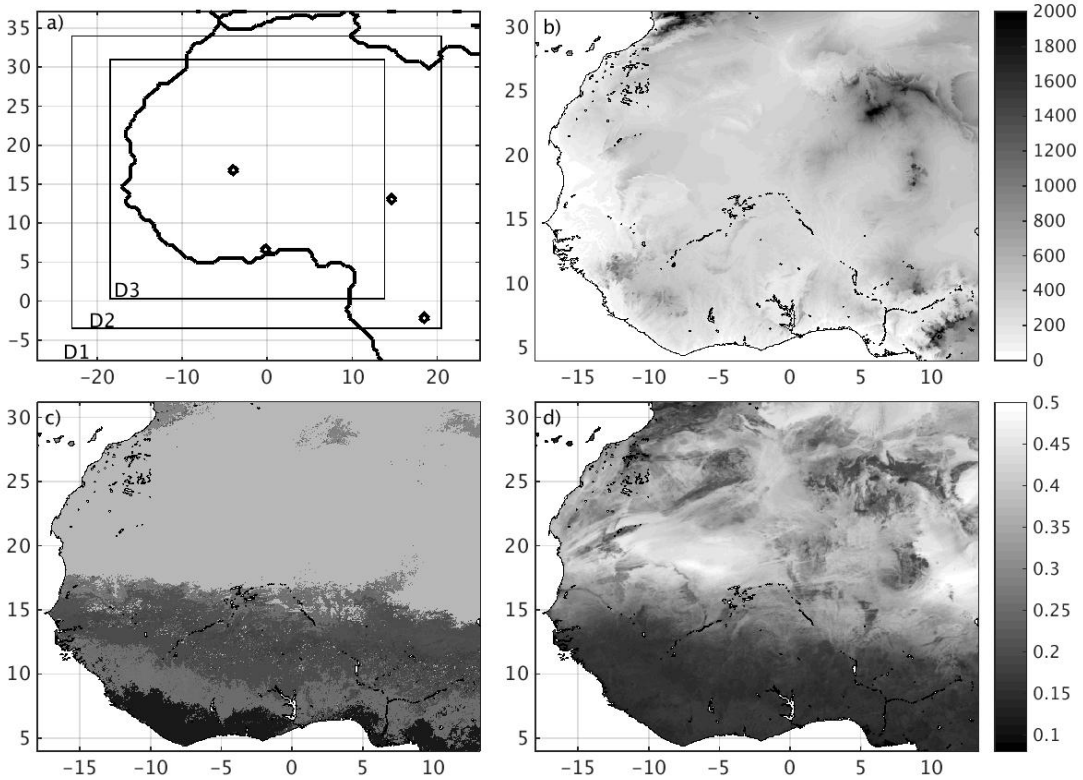

Figure 1. a) Model domain configuration, b) topography (meters) of inner domain (4 km grid-spacing), c) surface albedo as a function of vegetation, d) surface albedo from MODIS satellite data. MODIS albedo corresponds to July 2006 monthly mean.

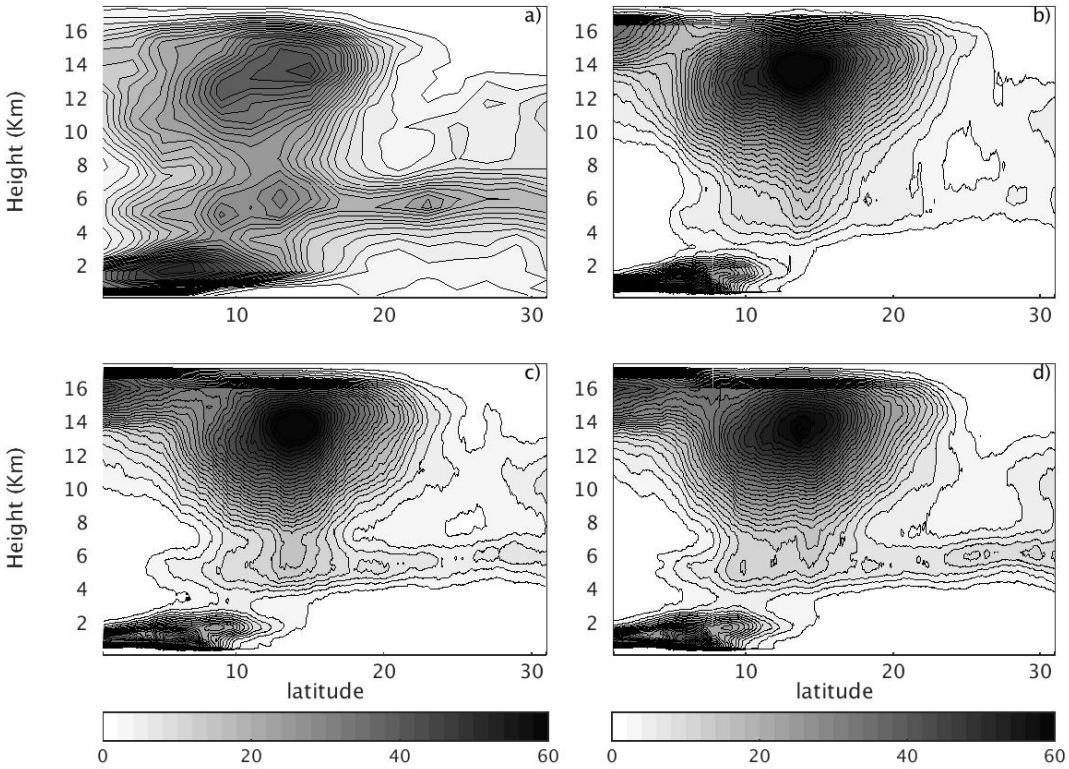

Figure 2. Zonal mean (averaged between 10°W-10°E) cloud fraction for July-September 2006 for a) CloudSat and Calipso satellite observations, b) 38Lev case, c) 87Lev case, d) 87Lev_MODIS case. All plots represent daily means and the contour interval is 2%.

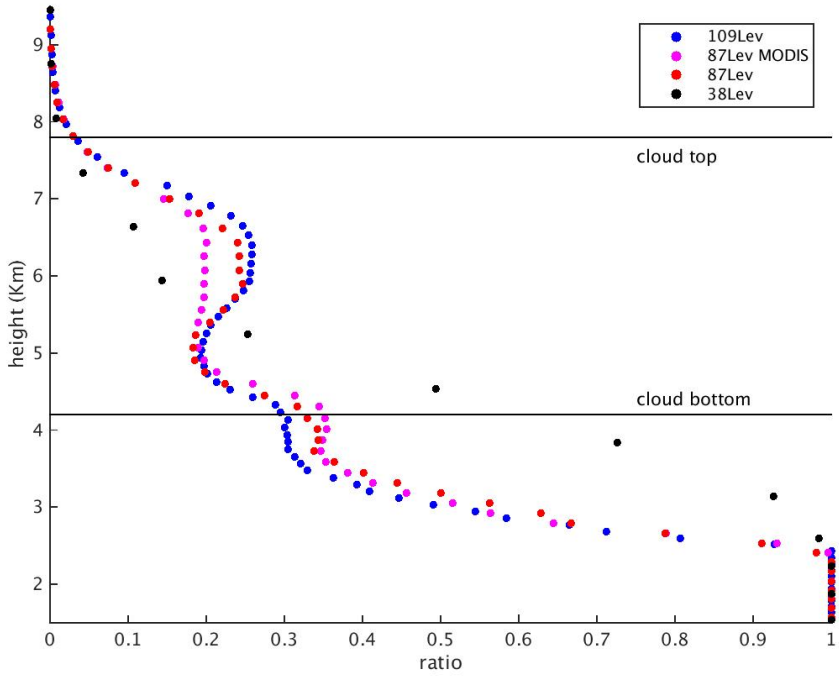

Figure 3. Vertical profile of ratio of liquid to liquid plus ice mixing ratio. The ratio has been averaged zonally (10°W-10°E), meridionally (24-29°N), daily and seasonally (JAS). Thin black lines roughly represent the average level of the top and bottom of the Saharan mid-level clouds.

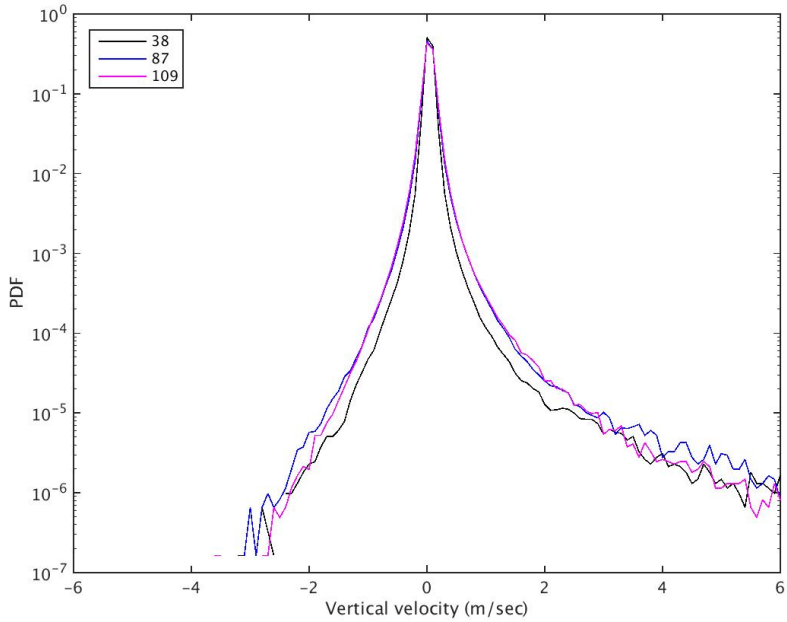

Figure 4. PDF of vertical velocity (m/sec) at 500hPa for 38 (black), 87 (blue) and 109 (magenta) vertical level simulation.

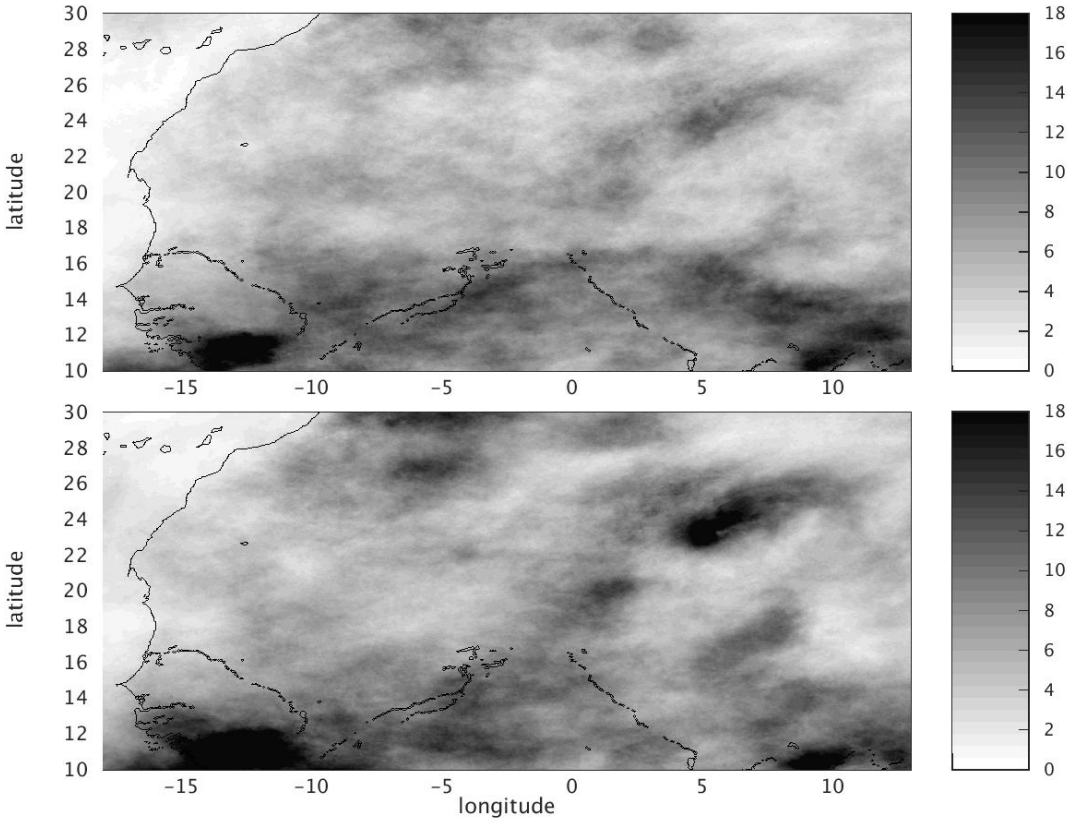

Figure 5. Simulated average cloud fraction from 600 to 400hPa for the month of July-September 2006 for 87Lev (top) and 87LevM (bottom) case. The cloud fraction has been averaged from 15:00 to 01:00 UTC, when the clouds have the largest extent.

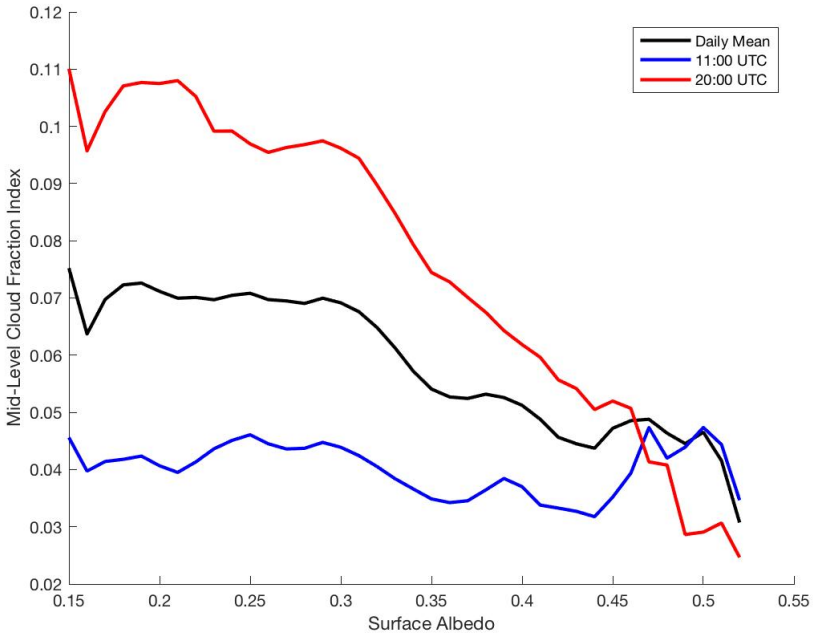

Figure 6. Histogram of vertically averaged cloud fraction as a function of surface albedo for 11:00 UTC, 20:00 UTC, and daily mean. The cloud fraction has been averaged within the mid-level cloud layer and for 10°W-10°E and 20°-30°N.

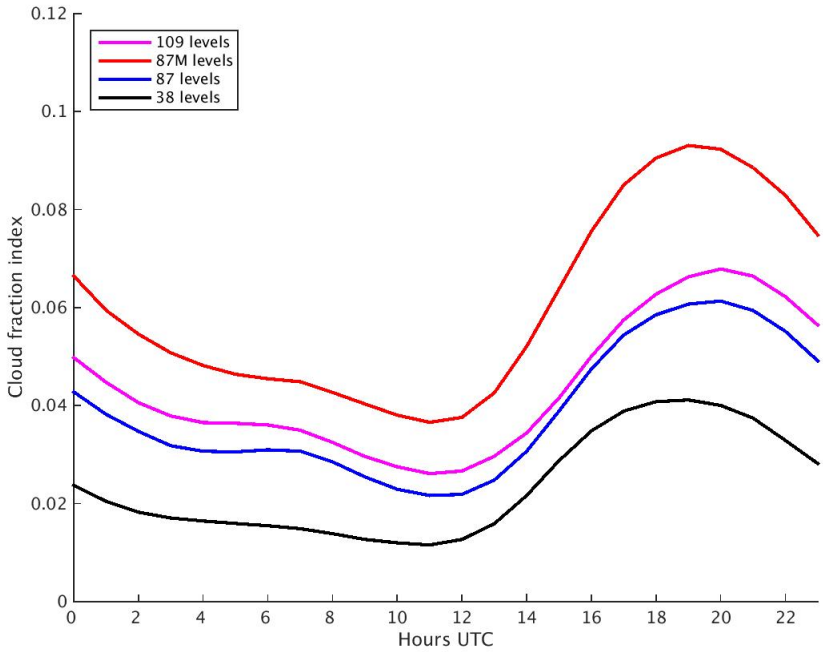

Figure 7. Diurnal cycle of the zonal mean mid-level cloud fraction averaged between 600-400hPa, 10°W-10°E, and 23°-27°N.

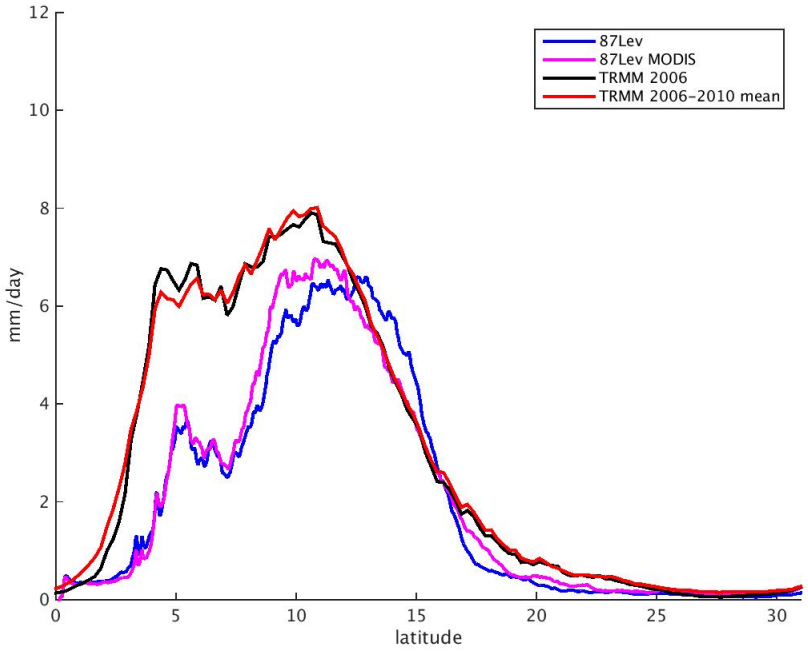

Figure 8. Zonal mean profile for precipitation during August 2006.

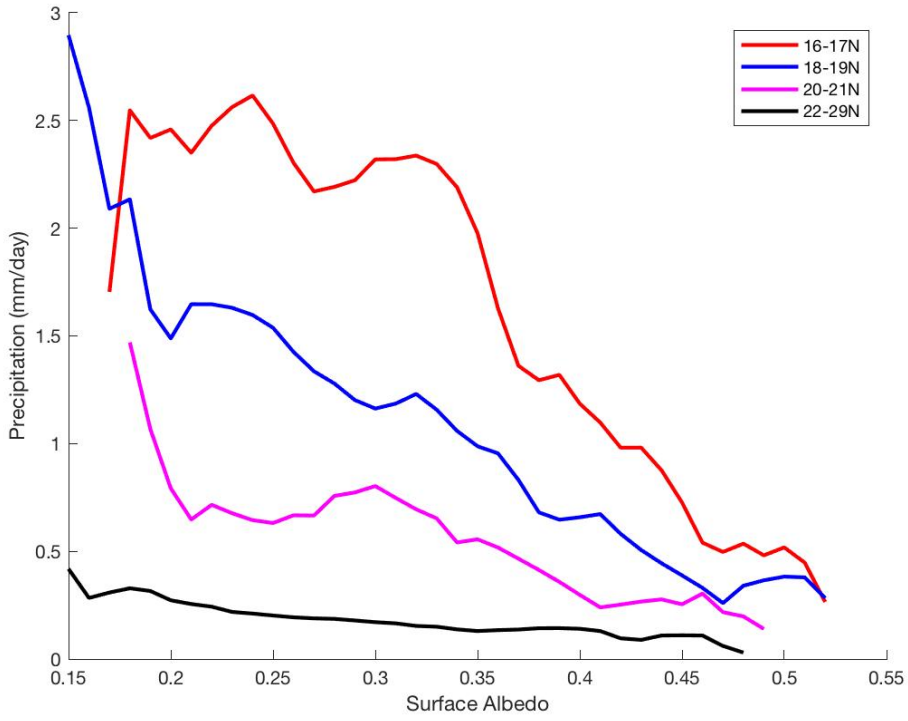

Figure 9. Histogram of daily mean precipitation (seasonally averaged, JAS) versus surface albedo for different latitudinal bands.